The Effect of Anodic Potential on Surface Layers of Chalcopyrite during Ammonia–Ammonium Chloride Leaching

Xiaoming Huaa, Yongfei Zheng, Qian Xu, Xionggang Lu, Hongwei Cheng, Xingli Zou, Qiushi Song, Zhiqiang Ning and Michael L. Free

Abstract The effect of the anodic polarization on the composition and morphology of the surface layer formed on chalcopyrite during ammonia–ammonium chloride leaching was investigated. The anodic polarization on the chalcopyrite electrode was used for oxidation and dissolution of chalcopyrite, and the resulting oxidized layers were characterized by XPS, SEM and optical microscopy. The results show that oxide layers exist on the chalcopyrite surface with or without any anodic polarization in the leaching solution at ambient atmosphere. However, the composition and morphology of the layers are strongly depended on the extent of polarization. The distribution of FeOOH and Fe_2O_3 within the oxidized layer was inhomogeneous for the sample at the open circuit potential (OCP). The composition and morphology of the oxidized layers which were formed at anodic potentials lower than 0.3 V versus SCE were similar to those of the chalcopyrite at the OCP. At anodic potentials above 0.4 V, the oxidized layers contained many cracks, and they were fragile and exfoliated. Furthermore, the sulfide had been oxidized to sulfur species with higher oxidation states. The oxidation of the chalcopyrite seemed to undergo a cyclically oxidative process that suggested growth and spallation of oxidation layers on chalcopyrite in a layer-by-layer sequence.

X. Huaa · Q. Song · Z. Ning
School of Materials Science and Engineering, Northeastern University, Shenyang 110004, People's Republic of China

Y. Zheng · Q. Xu (✉) · X. Lu · H. Cheng · X. Zou
State Key Laboratory of Advanced Special Steel, School of Materials Science and Engineering, Shanghai University, Shanghai 200072, People's Republic of China
e-mail: qianxu@shu.edu.com

M. L. Free
Department of Metallurgical Engineering, University of Utah, Salt Lake City, UT 84112, USA

Introduction

Chalcopyrite ($CuFeS_2$) is the most important mineral for production of metallic copper and its dissolution behavior represents the most important technological consideration in the hydrometallurgical extraction of copper. Hydrometallurgical copper extraction for low-grade chalcopyrite ores has been attracted much attention from many perspectives such as the ability to deal with a large spectrum of impurities, applicability to low-grade materials, and feasibility of low-capacity operation. Many lixiviants such as sulfates, chlorides and ammonia have been reported for copper leaching. Due to the slow leaching kinetics for chalcopyrite, there are many investigations on the mechanism of the oxidative dissolution of this mineral in order to understand the reason for slow dissolution rate. Although it is widely accepted that dissolution of chalcopyrite is retarded by the inhibition surface layers [1, 2], the surface chemistry during leaching has not been well understood till now. However, despite the enhanced understanding today, no universal agreement has been reached on the composition and microstructure of the inhibition layers, and the role of the layers during the leaching process.

The inhibition layer is less reactive than chalcopyrite, furthermore the compact layers form a barrier to lixiviant access by chalcopyrite, and thereby hinder dissolution. It can be concluded from the literature [3] that the composition of the passivation layers, which are the intermediate products, are dependent strongly on the anodic potential of the reactive chalcopyrite. A number of surface species in the layers have been proposed for the ammonia leaching system, such as Fe_2O_3 [4], iron-based precipitation layer [5] and $Cu_{1-x}FeS_2$ [6]. Despite some researches about the composition and morphology of the inhibition layer on the leached chalcopyrite [7], there is no study found about the correlation between morphology of the inhibition layers and the anodic potentials of the chalcopyrite. Since the variously anodic potentials on chalcopyrite can simulate the functions of different oxidants used in the oxidative leaching of chalcopyrite, this correlation is important to more completely understand the morphology of the inhibition layers and its relationship with the mechanism of passivation.

In this study, based on the voltammetry measurements, the dependence of composition and morphology of the passivation layers on the chalcopyrite with anodic polarization is presented in combination with XPS analyses and metallographic microscopy. Furthermore, the in-depth compositional profiles of the layers on the oxidized chalcopyrite were evaluated with XPS depth profiling. This information is critical to understanding the surface chemistry during chalcopyrite leaching.

Experimental

High-purity polycrystalline chalcopyrite samples were obtained from GuizhouProvince, China, and there was no impurity phases detected for the samples by XRD analysis. The samples (∅ 3 × 10 mm) were fabricated into cylindrical electrodes, mounted in epoxy resin holders, connected with copper wire using silver epoxy and polished with 2.5 μm diamond abrasive. All electrochemical measurements were driven by a BioLogicHCP-803 High Current Potentiostat, in a three-electrode system with the saturated calomel electrode (SCE) serving as a reference electrode, a graphite plate as a counter electrode, and a chalcopyrite electrode as the stationary working electrode. The electrolyte solution contained 1 M NH_4OH and 2 M NH_4Cl (pH ∼ 8.5) at 35 °C, and was no agitated and left to the open atmosphere.

After the potentiostatic polarization the samples were rinsed with deionized water, dried in air, and characterized with optical microscopy (OM, DM4000 M, Leica), scanning electron microscope (SEM, SU-1500, HITACHI), and X-ray photoelectron spectroscopy (XPS, Fisher Scientific, ESCALAB). Some samples presented in Fig. 3 were collected by adhesive tape to separating the layers from the bulk chalcopyrite. The in-depth composition analysis of the cubic sample, which was leached in the electrolyte solution at OCP, was carried out by alternating XPS measurements and Ar+ sputtering. The etching depth was detected from the profilometer (Dekta 840, Veecog) analyses, and an etching rate was about 0.1282 nm/s.

Results and Discussion

Figure 1 shows the linear sweep voltammograms in the electrolyte of 1 M NH_4OH and 2 M NH_4Cl at 35 °C for the chalcopyrite and platinum electrodes. The rest potential on the chalcopyrite electrode (shown in the inset (a) in Fig. 1) changes over time, probably because there are coupled redox reactions, such as those shown in Eqs. (1) and (2) as the presence of oxygen, with different kinetic rates.

$$4CuFeS_2(s) + 12OH^- = 4Fe(OH)_3 + CuS + S^° + 12e \qquad (1)$$

$$3[O_2] + 6H_2O + 12e^- = 12OH^- \qquad (2)$$
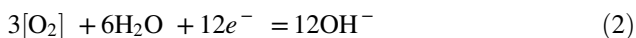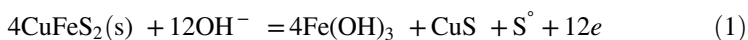
On the Pt electrode, the anodic current increased rapidly above 0.8 V due to oxygen evolution. The anodic features of the chalcopyrite electrode were illustrated between the rest potential and 0.7 V, which could be divided into two main potential regions. At potentials below 0.3 V, the anodic current density was very small and increased slowly. As the potential increased above 0.4 V, the current

Fig. 1 Linear sweep voltammograms with scanning rate of 20 mV/s in 1 M NH$_4$OH and 2 M NH$_4$Cl solution, solid line for the chalcopyrite electrode, dash line for platinum electrode. The inset figure (**a**) is the open circuit potential-time curve for the chalcopyrite electrode, and inset (**b**) is the assembly of chalcopyrite electrode
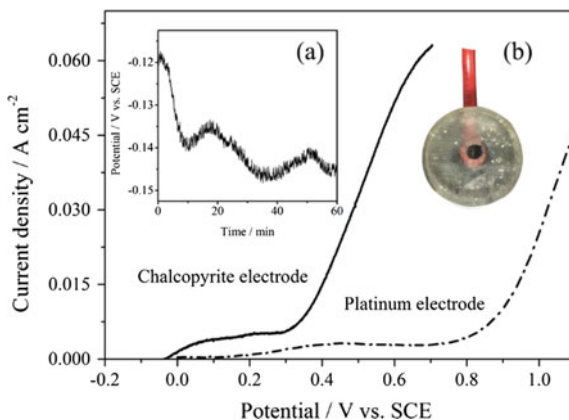
increased rapidly with the applied potential, and metal-depleted sulfide should be reduced and decomposed.

Figure 2a shows the changing optical characteristics of the chalcopyrite surface as a function of exposure in the electrolyte solution under ambient conditions at the OCP from 0 to 250 h. Because the release of Fe to oxyhydroxide phases is generally faster than Cu, the formation of covellite and metastable CuFe$_{1-y}$S$_{1-z}$ can be assumed in the subsurface. The brown-yellow surface is likely due to FeOOH and the blue one due to the formation of covellite The surface color changes should be dependent on the composition and thickness of the surface layer during oxidation. It can be deduced that the kinetics for chalcopyrite oxidation is quite slow in the electrolyte solution at OCP since the color change needs a relatively long time Furthermore there is no copper dissolved as mentioned by Moyo [7] in the ammonia solution open to the atmosphere.

Figure 2b shows XPS spectra measured for the 100-h leaching sample surface (Fig. 2) after sputtering the surface at different depths. The appearance of Fe–O (711.4 eV), O^{2-} and –OH (530.0, 531.4 eV) from the curves of Fe 2p and O 1s suggests that FeOOH is contained on the top layer. The atomic ratio of OH$^-$ to O^{2-} decreased from 1.3 to 0.6 corresponding to the initial surface and the surface that was sputtered for 400 s. It can be deduced that the distribution of FeOOH and Fe$_2$O$_3$ with the depth was inhomogeneous, and the composition of FeOOH reached a maximum at the top surface. The Fe–O was totally removed and substituted by Fe–S after the third sputter cycle according to the Fe 2p and O 1 s spectra. The surface layer containing of FeOOH and Fe$_2$O$_3$ should be thinner than 180 nm based on an estimated etch rate of 0.1282 nm/s and a time of 1400 s. There were no sulfur and copper signals detected from S 2p and Cu 2p spectra on the top surface although the blue color of the sample was ascribed to covellite. However, the spectra of Cu 2p and Fe 2p showed that some Fe atoms and almost all Cu atoms were associated with sulfur after the first sputter cycle. The S 2p spectra presented
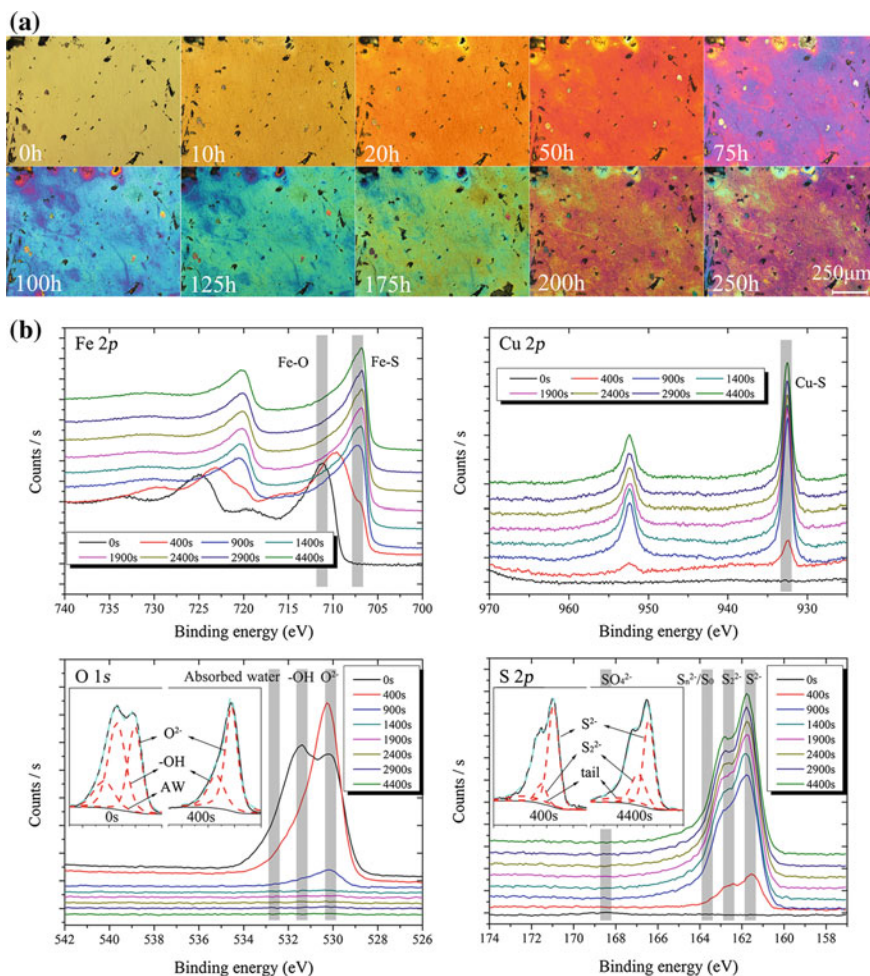
Fig. 2 **a** Optical microscopy photographs of the surface with leaching from 0 to 250 h under 1 M NH$_4$OH and 2 M NH$_4$Cl solution at 35 °C. **b** XPS depth (shown as sputtering time analysis of the sample leached for 100 h (shown as sputtering time with an estimated etch rate of 0.1282 nm/s)

in Fig. 2b consisted of two major doublets representing monosulfide and disulfide. The presence of S$_2^{2-}$ on the surface after the first sputter cycle suggests iron atoms were removed from the chalcopyrite and formed the oxide, then S^{2-} was oxidized to S$_2^{2-}$.

Figure 3 shows the current–time transients and the digital photos of the sample surface for the chalcopyrite electrodes at the potentials from 0.01 to 0.7 V for 5 h, respectively. It was observed that the anodic current density was near to zero when

Fig. 3 Potentiostatic polarization of chalcopyrite electrode with the corresponding optical microscopy photographs under 1 M NH₄OH and 2 M NH₄Cl solution
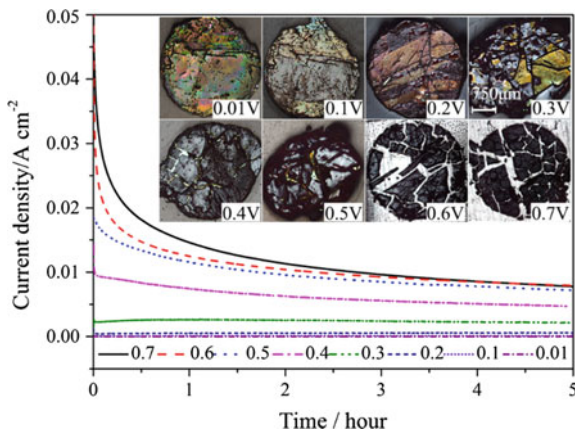
the anodic potential was lower than 0.2 V, and few changes occurred on the sample surface according to the color and integrity of the associated samples. When the anodic potential increased up to 0.4 V, and higher to 0.7 V, the anodic current increased depending on the potential applied. The chalcopyrite surface was covered by black layers with more cracks. The black layers were fragile and easily exfoliated from the bulk chalcopyrite.

Figure 4 shows the XPS spectra for the electrodes applied at different anodic potentials indicated in the figure legends. All spectra had a strong peak of Fe 2p3/2 at 711.1 eV that suggests the existence of $FeOOH/Fe_2O_3$ in the layers. At the anodic potentials lower than 0.4 V, the typical peaks of Cu 2p and S 2p spectra could not be detected, which means there are almost no Cu and S on the surface for the inadequate oxidation due to lowly anodic potentials. In addition, the feature of the XPS spectra for these samples was similar to those at the OCP. The results imply that the dissolution process on the electrode with the potential lower than 0.3 V was almost the same as the situation at OCP. When the potential increases up to 0.5 V or higher, some peaks assigned to Cu–O (934.8 eV) and Cu–S (932.5 eV) appeared in Cu 2p spectra, and the intensity of peaks assigned to S^{2-}/S^0, SO_4^{2-} increased, which confirms that S^{2-} can be oxidized to S^{+6} at the anodic potential higher than 0.5 V, and it can lead to dissolution of chalcopyrite.

Figure 5 shows the surface changes of the chalcopyrite electrode at the anodic potential of 0.4 V for varied times from 0 to 45 s. The surface color changing was drastically faster at 0.4 V compared with that at OCP. The surface morphology of the electrode after the anodic polarization for 45 s shown in Fig. 5b illustrates that the product layer (FeOOH) exfoliated from the bulk chalcopyrite (Fig. 3), and the underlayer (Cu sulfides or even the chalcopyrite) had been exposed.
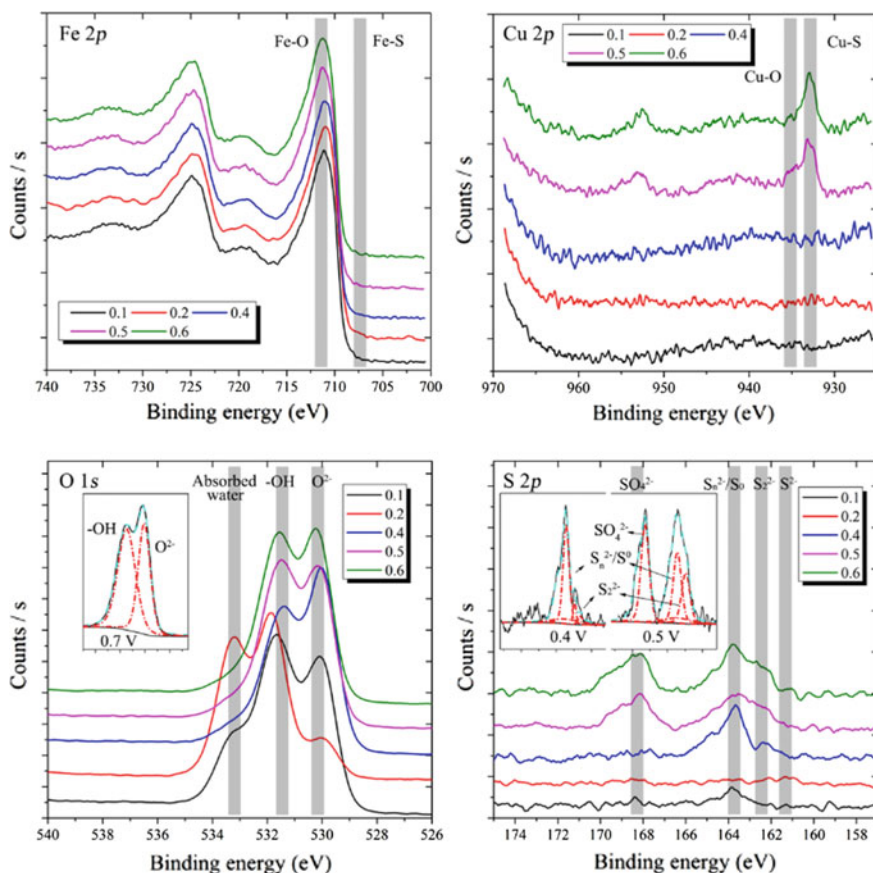
Fig. 4 Comparison of Fe 2p, Cu 2p, O 1s and S 2p peaks of the layers separated from the surface of chalcopyrite electrode under the different polarizations for 5 h
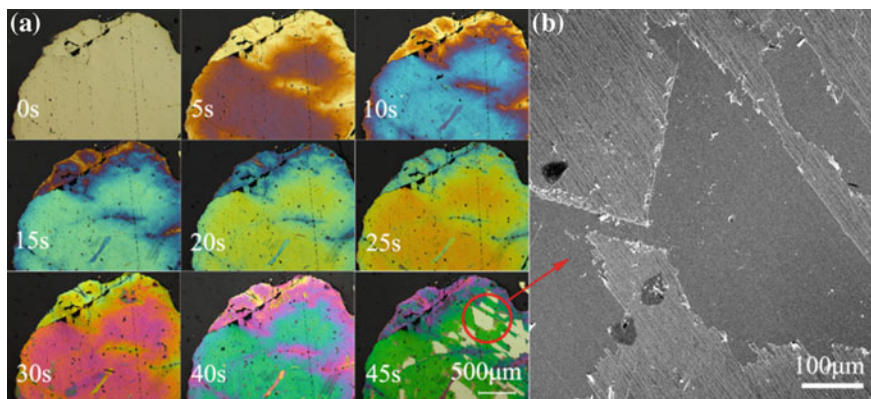

Fig. 5 **a** Optical microscope photograph of electrode surface at the anodic potential of 0.4 V for different times and **b** SEM image of the sample for 45 s

Conclusions

Oxidation reactions on the chalcopyrite electrode at the OCP occurred in the electrolyte solution of 1 M NH_4OH and 2 M NH_4Cl at 35 °C. The distribution of FeOOH and Fe_2O_3 with the depth in the oxidized layer was inhomogeneous, and there was accumulation of FeOOH at the top surface based on the XPS results. When the anodic potentials were lower than 0.3 V, the anodic polarization had little effect on the composition and morphology of the oxidized layers formed due to the oxidation of the chalcopyrite electrode compared with those of the chalcopyrite at the OCP. When increased up to 0.4 V, and even higher to 0.7 V, the rate of chalcopyrite oxidation increased dramatically, and the product layers with cracks were fragile and easily exfoliated from the bulk chalcopyrite. The sulfide can be oxidized to sulfur species with higher oxidation states. Furthermore, the oxidation of the chalcopyrite seemed to undergo a cyclically oxidative process that results in exfoliation of the oxide layer that exposes the bulk chalcopyrite in a layer-by-layer sequence.

References

1. Biegler T, Horne MD (1985) The electrochemistry of surface oxidation of chalcopyrite. J Electrochem Soc 132(6):1363
2. Li Y, Kawashima N, Li J, Chandra AP, Gerson AR (2013) A review of the structure, and fundamental mechanisms and kinetics of the leaching of chalcopyrite. Adv Colloid Interface Sci 197–198:1–32
3. Yi Q, Kelsall GH, Vaughan DJ, England KER (1995) Atmospheric and electrochemical oxidation of the surface of chalcopyrite ($CuFeS_2$). Geochim Cosmochim Acta 59(6): 1091–1100
4. Beckstead L, Miller J (1977) Ammonia, oxidation leaching of chalcopyrite-surface deposit effects. Metall Mater Trans B 8(1):31–38
5. Moyo T, Petersen J, Franzidis JP, Nicol MJ (2015) An electrochemical study of the dissolution of chalcopyrite in ammonia–ammonium sulphate solutions. Can Metall Q 3:368–327
6. Warren G, Wadsworth M (1984) The electrochemical oxidation of chalcopyrite in ammoniacal solutions. Metall Mater Trans B 15(2):289–297
7. Moyo T, Petersen J (2016) Study of the dissolution of chalcopyrite in solutions of different ammonium salts. SAIMM J 116(6): 509–516, 279–288